



Article

Computational Analysis of Nanoparticle Shapes on Hybrid Nanofluid Flow Due to Flat Horizontal Plate via Solar Collector

Muhammad Imran ¹, Sumeira Yasmin ¹, Hassan Waqas ^{1,*}, Shan Ali Khan ¹, Taseer Muhammad ², Nawa Alshammari ³ , Nawaf N. Hamadneh ^{3,*} and Ilyas Khan ⁴

¹ Department of Mathematics, Government College University, Faisalabad 38000, Pakistan; drmimranchaudhary@gmail.com (M.I.); yasmeensumaira.1122@gmail.com (S.Y.); shazukhan1214@gmail.com (S.A.K.)

² Department of Mathematics, College of Sciences, King Khalid University, Abha 61413, Saudi Arabia; tasgher@kku.edu.sa

³ Department of Basic Sciences, College of Science and Theoretical Studies, Saudi Electronic University, Riyadh 11673, Saudi Arabia; n.alshammari@seu.edu.sa

⁴ Department of Mathematics, College of Science Al-Zulfi, Majmaah University, Al-Majmaah 11952, Saudi Arabia; i.said@mu.edu.sa

* Correspondence: hassanwaqas22@gcuf.edu.pk (H.W.); nhamadneh@seu.edu.sa (N.N.H.)

Abstract: The present work discusses the 2D unsteady flow of second grade hybrid nanofluid in terms of heat transfer and MHD effects over a stretchable moving flat horizontal porous plate. The entropy of system is taken into account. The magnetic field and the Joule heating effects are also considered. Tiny-sized nanoparticles of silicon carbide and titanium oxide dispersed in a base fluid, kerosene oil. Furthermore, the shape factors of tiny-sized particles (sphere, bricks, tetrahedron, and platelets) are explored and discussed in detail. The mathematical representation in expressions of PDEs is built by considering the heat transfer mechanism owing to the effects of Joule heating and viscous dissipation. The present set of PDEs (partial differential equations) are converted into ODEs (ordinary differential equations) by introducing suitable transformations, which are then resolved with the *bvp4c* (shooting) scheme in MATLAB. Graphical expressions and numerical data are obtained to scrutinize the variations of momentum and temperature fields versus different physical constraints.

Keywords: second grade hybrid nanofluid; entropy generation; thermal radiation; solar collector; nanoparticle shapes; *bvp4c*; MATLAB



Citation: Imran, M.; Yasmin, S.; Waqas, H.; Khan, S.A.; Muhammad, T.; Alshammari, N.; Hamadneh, N.N.; Khan, I. Computational Analysis of Nanoparticle Shapes on Hybrid Nanofluid Flow Due to Flat Horizontal Plate via Solar Collector. *Nanomaterials* **2022**, *12*, 663. <https://doi.org/10.3390/nano12040663>

Academic Editor: Mikhail Sheremet

Received: 8 December 2021

Accepted: 1 February 2022

Published: 16 February 2022

Publisher's Note: MDPI stays neutral with regard to jurisdictional claims in published maps and institutional affiliations.



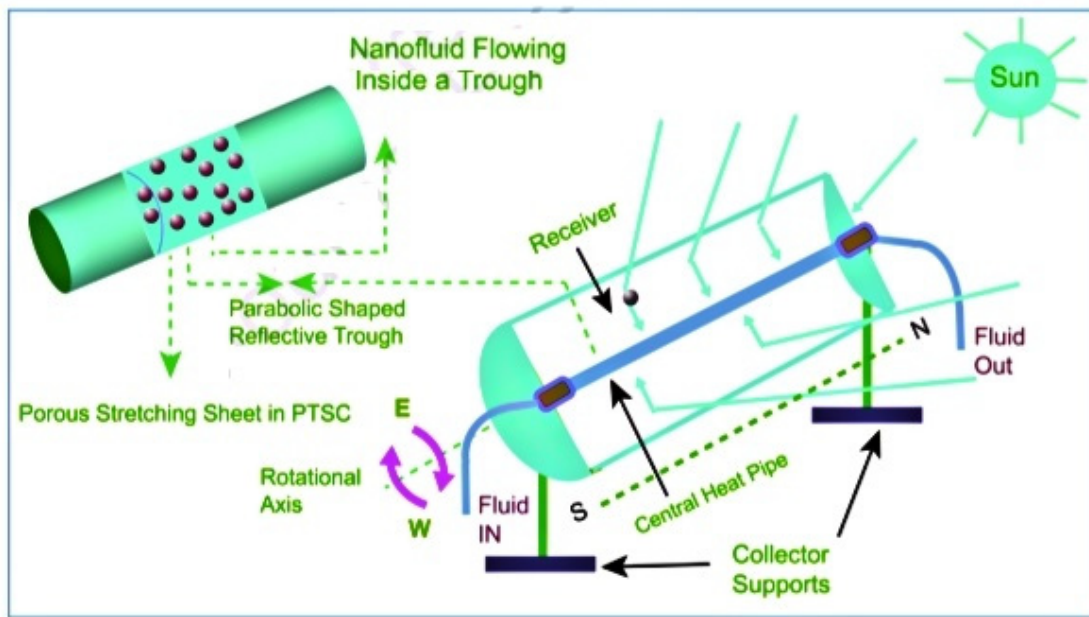
Copyright: © 2022 by the authors. Licensee MDPI, Basel, Switzerland. This article is an open access article distributed under the terms and conditions of the Creative Commons Attribution (CC BY) license (<https://creativecommons.org/licenses/by/4.0/>).

1. Introduction

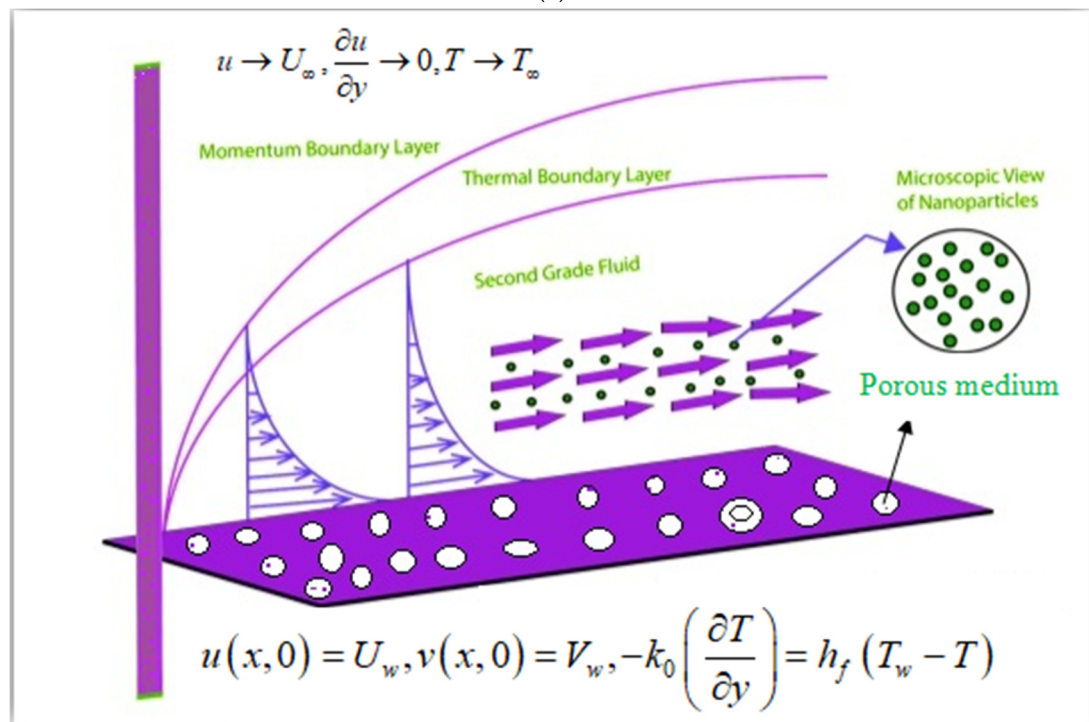
Nanoparticles are commonly employed in food, medication, nuclear power stations, agriculture, and other applications. Such fluids are created from the continuous dispersion of nano-sized particles in base fluids including water, ethylene glycol, lubricating oils, blood, or other fluids, and are termed as nanofluids. Hybrid nanofluids are formed by the dispersion of two or more components in the given base fluid. Such fluids have numerous applications in medicine research and technology. The majority of medications are manufactured as hybrid nanofluids, and blood is utilized as a research base fluid to assess the chemical interactions of the compounds in the blood. In addition, the hybrid-type nanofluids are employed to improve the thermal efficiencies of base fluids. Correct viscosities as well as temperatures are necessary to maintain the consistency of blood transfer for improved blood circulation. To improve the thermal properties of these fluids, nano-scale particles are dispersed in the base liquid, which improves the thermal attributes. Choi [1] has developed a comprehensive strategy for increasing the heat transfer rate of these fluids. Nanofluids are fluids with increased thermophysical characteristics. Choi's pioneering study was motivated by the observation that base fluids with lower thermal conductivity are inefficient for industrial heat transfer applications. Chemicals, metals such

as (*Cu*, *Al* and *Ag*), metallic compounds (*SiC*), metallic oxides (silica oxides, alumina oxides, and zirconia oxides), and nitrides are among the nanometer-sized particles that contribute to nanofluids. Nanofluids are classified into four types based on their natural environment and quantity: (i) nanofluids for pollution purifying (agricultural), (ii) nanofluids for heat transfer, (iii) nanofluids for drug delivery (healthcare fields), and (iv) pharmaceutical nanofluids with multiple effects in fields such as oncology, microbiology, and cardiology. Rasool et al. [2] explored the Marangoni convection in Casson-based nanofluid flow when impacted by the existence of Lorentz forces. Mahanthesh et al. [3] discovered the consequences of the quadratic thermal radiated effect and the quadratic Boussinesq assumptions on the heat transmission of 36 nano-sized nanoparticles across a vertical surface. Ramzan et al. [4] evaluated the magneto Casson-type nanofluid with a changing heat source/sink as well as modified Fourier's and Fick's laws (FFLs) across a stretched cylinder. Eid et al. [5] identified the hydrothermal differences of viscous and elastic nanofluid flows in a porosity medium through a stretched surface. The behavior of Fourier's and Fick's laws on nanofluid flow was scrutinized by Gowda et al. [6]. Alsabery et al. [7] disclosed the convection phenomenon in nanofluid flow. Alsabery et al. [8] investigated the forced convection heat transformer through horizontal channels. Nanofluid investigation has been further addressed in different recent works [9–12].

A solar energy collector (SEC) (see Figure 1a) is defined as a heat transfer mechanism that absorbs and transforms solar radiation into heat, which is then transported to a fluid (commonly H_2O , air, or lubricant) that moves via an SC (solar collector). Electric energy for manufacturing purposes necessitates the use of large capacity solar collectors. However, the mechanism is inefficient due to poor heat transport. As a consequence, a great deal of study has been conducted in fields including heat pumps, hot water services, cooling, and manufacturing processes. Solar energy is a natural and abundant source of energy. Due to the tremendous utility of solar energy, it is employed in implementations such as solar collectors. The implementations of nanofluids to enhance the efficiency of solar thermal collectors over standard Newtonian fluids are well established within research. Hayat et al. [13] reported the three-dimensional second grade boundary layer flow of nanofluids through a stretched plate including thermal radiation with a heat source/sink effect. Waqas et al. [14] considered the bio-convective thermal radiative impact in Darcy–Forchheimer nanofluid flow with Wu's slip through an expanding cylinder/plate. Wakif et al. [15] scrutinized the thermal radiation impact on aluminum–copper oxide hybrid-based nanofluids. Hussain et al. [16] assessed the heat transformer characteristics of MHD (magnetohydrodynamic) with hybrid-based nanofluid flow in the existence of thermal radiation effects. Kerschbaumer et al. [17] established that radiation refrigeration is a relevant issue for applications in thermal management of buildings as well as energy conservation. Alsabery et al. [18] discussed the dual phase nanofluid in a 3D solar collector. Han and Chen [19] discussed the micro-nanofluidic preconcentrator through a microchannel. Han and Chen [20] discussed the implementations of ion transport in micro-nanofluidic mechanisms. Waqas et al. [21] investigated the bioconvective flow of cross nanofluid in the presence of activation energy. Han and Chen [22] discussed viscous nanofluids in microchannels. The graphical representation is elucidated in Figure 1a.



(a)



(b)

Figure 1. Cont.

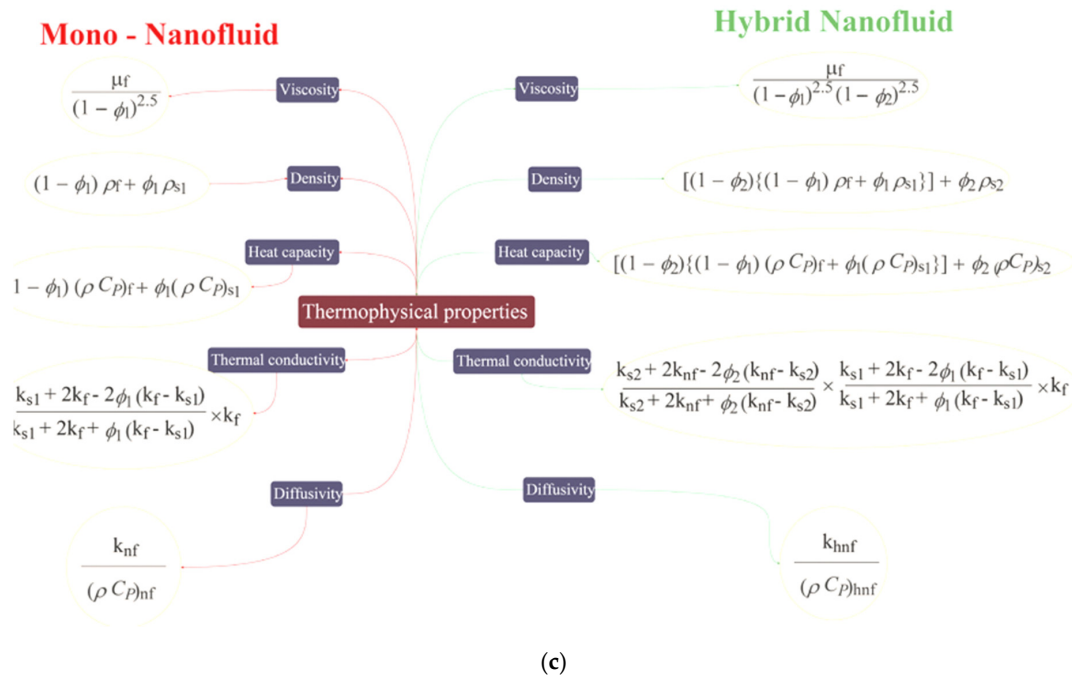


Figure 1. (a) solar collector system with representation, (b) schematic of flow problem, and (c) thermophysical properties of nanofluid and hybrid nanofluid.

In recent decades, researchers and engineers have placed considerable attention on entropy generation. Due to their significance, the characteristics and importance of entropy in various industry applications such as electrical heaters, refrigerators, combustion generators, have been investigated in the context of most aspects of heat phenomena. Entropy generation minimization is a method for modeling and optimizing equipment that have (thermodynamic) inefficiencies because of several properties, such as fluid flow viscous dissipation. As a result, for more advantageous execution of any structure, the conditions that would be effective in entropy generation depreciation should be identified. Entropy generation investigation is useful in analyzing the reliability of electrical or mechanical devices. Fluid dynamics include a combination of fundamental irreversible behavior, fluid viscosity with mechanism, and Joule heating, etc. Eid et al. [23] explored the 2D cross nanofluid flow through a linearly stretchy surface with a magnetic field in the Darcy–Forchheimer permeable regime. Eid et al. [24] examined the carbon nanotubes CNT’s suspending magnetohydrodynamics flow of micropolar dusty nanoparticles impinging on a porous extended surface inserted in a porous regime. Turkyilmazoglu et al. [25] characterized the velocity slip effect and entropy generation in thermal radiative transportation via a metal porous channel. Shehzad et al. [26] investigated how the heat flow in microchannels involving entropy generation can be useful in many implementations including micro-aircrafts, mechanical–electromechanical solutions, electrical device refrigeration, and micro-heat transfer mechanisms. Hayat et al. [27] analyzed the Carreau nanofluid flow with entropy generation.

From the above discussed literature and other similar research, the authors of the current research observed that few studies are available of second grade hybrid nanofluid flow (HNF) through a stretched surface. The current work aims to clarify the impacts of nanoparticle shape factors on second grade hybrid nanofluid over a flat horizontal porous surface with entropy generation. The significance of thermal radiation and viscous dissipation on heat equation is scrutinized. The velocity slip and convective heat transfer are also analyzed. The nanoparticles silicon carbide *SiC* and titanium oxide *TiO₂* are involved in kerosene oil-based fluids to improve the heat transfer. In the current research, the bvp4c tool in MATLAB is used to find the solution. This crucial research may help to enhance industrial production, especially in the solar energy collector sectors. This

research is more applicable in the field of heat transfer, and current outcomes may be more effective in nanotechnology and biomedical fields such as drug delivery and cancer treatment. Therefore, such computational analysis is attractive to researchers.

2. Mathematical and Physical Descriptions

Here, we consider the steady, two-dimensional second grade laminar flow with a hybrid-type nanofluid model across a stretched porous surface in the existence of different nanoparticle shapes. Furthermore, the effects of radiative heat flux in the occurrence of a viscous dissipation effect and Joule heating are addressed. Moreover, the magnetic field is examined. The entropy of system is also involved in the current study. The present model was sketched with mathematical characteristics which indicate the fluid velocity, held smooth, and the stretching surface under the irregular extending rate:

$$U_w(x, t) = bx, \quad (1)$$

where b represents the preliminary extendable rate of a stretched porous surface. The isolated temperature of a flat surface is symbolized by $T_w(x, t) = T_\infty + b^*x$ and it is considered that its suitability is constant in supposition at $x = 0$, $(b^*, T_w \& T_\infty)$, describing the thermal variation rate as well as fluid temperature of wall and ambient temperature respectively.

Additionally, the stress-tensor of Williamson nanofluids is expressed as:

$$S^* = \mu A_{\zeta 1} + \alpha_1 A_{\zeta 2} + \alpha_1 A_{\zeta 1}^2 - pI, \quad (2)$$

where the additional stress tensor in a second grade is symbolized by A_{ij} and, mathematically, the form is expressed as:

$$\begin{aligned} A_{\zeta 1} &= (\text{grad } V) + (\text{grad } V)^T, \\ A_{\zeta 2} &= \frac{dA_{\zeta 1}}{dt} + A_{\zeta 1}(\text{grad } V) + A_{\zeta 1}(\text{grad } V)^T, \end{aligned} \quad (3)$$

where $(\alpha_1 \& \alpha_2)$ represents the material variables. μ is denoted by the fluid dynamic viscosity, p represents the pressure, I explains the identity tensor, $(A_{\zeta 1} \& A_{\zeta 2})$ both demonstrate the Rivlin–Erickson tensors, $\frac{d}{dt}$ expresses the time-dependent derivative, and the fluid velocity is signified by V . We prove the Clausius–Duhem inequality. Furthermore, we determine that the Helmholtz unlimited temperature is the minutest in equipoise for the liquid flow closed by at rest when:

$$\mu \geq 0, \alpha_1 \geq 0, \alpha_1 + \alpha_2 = 0$$

If $\alpha_1 + \alpha_2 = 0$, then the second grade nanofluid expression is diminishable from the viscous fluid. Figure 1b shows a graphical demonstration of the current theoretical observation.

2.1. Governing Equations

The flow problem which involves the set of governing equations, such as velocity and temperature, is expressed as [28,29]:

$$\frac{\partial u}{\partial x} + \frac{\partial v}{\partial y} = 0, \quad (4)$$

$$\begin{aligned} u \frac{\partial u}{\partial x} + v \frac{\partial u}{\partial y} &= U_\infty \frac{dU_\infty}{dy} + \frac{\alpha_1}{\rho_{hmf}} \left[\frac{\partial u}{\partial x} \left(\frac{\partial^2 u}{\partial y^2} \right) + u \left(\frac{\partial^3 u}{\partial x \partial y^2} \right) + \frac{\partial u}{\partial y} \left(\frac{\partial^2 v}{\partial y^2} \right) + v \left(\frac{\partial^3 u}{\partial y^3} \right) \right] \\ &+ \frac{\mu_{hmf}}{\rho_{hmf}} \left(\frac{\partial^2 u}{\partial y^2} \right) - \frac{\mu_{hmf}}{\rho_{hmf} k} u, \end{aligned} \quad (5)$$

$$u \frac{\partial T}{\partial x} + v \frac{\partial T}{\partial y} = \frac{k_{hmf}}{(\rho C_p)_{hmf}} \left(\frac{\partial^2 T}{\partial y^2} \right) - \frac{1}{(\rho C_p)_{hmf}} \left(\frac{\partial q_r}{\partial y} \right) + \frac{\mu_{hmf}}{(\rho C_p)_{hmf}} \left(\frac{\partial u}{\partial y} \right)^2 + \frac{\sigma_{hmf} B^2(t) u^2}{(\rho C_p)_{hmf}}. \quad (6)$$

with boundary conditions:

$$\begin{aligned} u(x, 0) &= U_w, v(x, 0) = V_w, T = T_w, \\ u &\rightarrow U_\infty, \frac{\partial u}{\partial y} \rightarrow 0, T \rightarrow T_\infty \text{ as } y \rightarrow \infty. \end{aligned} \tag{7}$$

In the above equations, the components of velocity are denoted by $(u&v)$ along the $(x&y)$ direction respectively, the dynamic viscosity of second grade hybrid nanofluid is μ_{hnf} , (ρ_{hnf}) represents the hybrid nanofluid density and k_{hnf} shows the hybrid nanofluid thermal conductivity (see Table 1). Furthermore, q_r considers the thermal radiative heat flux, $(\rho C_p)_{hnf}$ describes the specific heat capacitance of nanofluid, and the porous stretchable surface characterized by V_w .

Table 1. Thermophysical properties of base fluid with nanoparticles.

Physical Characteristics	Kerosene Oil	SiC	TiO ₂
$C_p / JKg^{-1}K^{-1}$	2090	1340	686.2
ρ / Kgm^{-3}	783	3370	4250
$k / Wm^{-1}K^{-1}$	0.15	150	8.9638
$\sigma / \Omega^{-1}m^{-1}$	5×10^{-11}	–	2.38×10^6

Here, hnf explains the thermophysical aspect of the nanofluid, the solid particles are shown as $s1, s2$, the base fluid is represented as f , and the solid volume fraction nominated by ϕ_1, ϕ_2 utilizing the nanoparticles. The thermal conductivity in case of shape factors is addressed as:

$$k_{hnf} / k_{gf} = \left[\left((k_{s1} + (m - 1)k_{gf}) - (m - 1)\phi_2(k_{gf} - k_{s2}) \right) / \left((k_{s2} + (m - 1)k_{gf}) - \phi_2(k_{gf} - k_{s2}) \right) \right].$$

Here, $k_{gf} / k_f = \left[\left((k_{s1} + (m - 1)k_f) - (m - 1)\phi_1(k_f - k_{s1}) \right) / \left((k_{s1} + (m - 1)k_f) - \phi_1(k_f - k_{s1}) \right) \right].$

2.2. Calculation of Rosseland Approximation

The Rosseland approximation by Brewster [30] can be expressed as:

$$q_r = -\frac{4\sigma^*}{3k^*} \frac{\partial T^4}{\partial y}, \tag{8}$$

where, σ^* illustrates the Stefan–Boltzmann constant and k^* stands for the mean absorption coefficient.

2.3. Similarity Transformations

The similarity transformation for PDEs which are converted into ODEs is addressed as:

$$\zeta(x, y) = \sqrt{\frac{b}{v_f}} y, u = bx f'(\zeta), v = \sqrt{v_f b} f(\zeta), \theta(\zeta) = \frac{T - T_\infty}{T_w - T_\infty}. \tag{9}$$

2.4. Resulting Equations

After applying the similarity transformations to the variables, the dimensional equations are reduced into dimensionless equation as follows:

$$f''' + A^2 + \Phi_1 \left[\Phi_2 (ff'' - f'^2) + \Gamma (2f' f''' - f''^2 - f f^{iv}) - \frac{K f'}{\Phi_1} \right] = 0, \tag{10}$$

$$\theta'' \left(1 + \frac{1}{\Phi_5} Pr Nr \right) + Pr \frac{\Phi_3}{\Phi_5} \left(f \theta' - f' \theta + \frac{Ec}{\Phi_1 \Phi_3} f''^2 + \frac{\Phi_4}{\Phi_3} M.Ec. f'^2 \right) = 0, \tag{11}$$

with B.C.

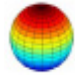



$$\begin{aligned} f(0) = S, f'(0) = 1, \theta(0) = 1, \\ f'(\zeta) \rightarrow A, f''(\zeta) \rightarrow 0, \theta(\zeta) \rightarrow 0, \text{ as } \zeta \rightarrow \infty. \end{aligned} \tag{12}$$

Here, ϕ_i 's is $1 \leq i \leq 5$ in the velocity and temperature equation of second grade hybrid nanofluid.

$$\begin{aligned} \Phi_1 &= (1 - \phi_1)^{2.5} (1 - \phi_2)^{2.5}, \Phi_2 = (1 - \phi_2) \left((1 - \phi_1) + \phi_1 \frac{\rho_{s1}}{\rho_f} \right) + \phi_2 \frac{\rho_{s2}}{\rho_f}, \\ \Phi_3 &= (1 - \phi_2) \left((1 - \phi_1) + \phi_1 \frac{(\rho C_p)_{s1}}{(\rho C_p)_f} \right) + \phi_2 \left(\frac{(\rho C_p)_{s2}}{(\rho C_p)_f} \right), \Phi_4 = \frac{\sigma_{hnf}}{\sigma_f}, \\ \Phi_5 &= \left(\frac{(k_{s2} + (m-1)k_{gf} - (m-1)\phi_2(k_{gf} - k_{s2}))}{(k_{s2} + (m-1)k_{gf} + \phi_2(k_{gf} - k_{s2}))} \right) \left[\frac{\begin{pmatrix} k_{s1} + (m-1)k_f \\ -\phi_1(k_f - k_{s1}) \end{pmatrix}}{\begin{pmatrix} k_{p1} + (m-1)k_f \\ -(m-1)\phi_1(k_f - k_{s1}) \end{pmatrix}} \right]. \end{aligned} \tag{13}$$

In Table 2, the geometrical form of nanoparticle shapes, their size, and sphericity are discussed in detail.

Table 2. Geometrical manifestation of tiny-sized particles with their size and sphericity.

Nanoparticle Shape	Geometrical Appearance	Size	Sphericity
Sphere		3.0	1.0
Tetrahedron		4.0613	0.82
Bricks		3.7	0.81
Platelets		5.7	0.52

2.5. Non-Dimensional Parameters

The derivatives are signified with respect to ζ . The velocity ratio parameter, non-Newtonian second grade parameter, magnetic parameter, porous parameter, Prandtl number, thermal diffusivity, thermal radiation parameter, Eckert number, and suction/injection parameter are defined as follows:

$$\left[\begin{aligned} A &= \frac{a}{b} \Gamma = \frac{\alpha_1 b}{\mu_f}, M = \frac{\sigma_f B_0^2}{c \rho_f}, K = \frac{\nu_f}{bk}, Pr = \frac{\nu_f}{\alpha_f}, \alpha_f = \frac{\kappa_f}{(\rho C_p)_f}, \\ Nr &= \frac{16\sigma^* T_\infty^3}{3\kappa^* \nu_f (\rho C_p)_f}, Ec = \frac{U_w^2}{(T_w - T_\infty)(C_p)_f}, S = -V_w \sqrt{\frac{1}{b\nu_f}}. \end{aligned} \right] \tag{14}$$

2.6. Physical Industrial Interest

In the present segment, the local skin friction coefficient and the heat transfer rate (local Nusselt number) of the flow problem are as follows:

$$C_f = \frac{\tau_w}{\rho_f U_w^2}, \quad Nu_x = \frac{xq_w}{k_f(T_w - T_\infty)}, \tag{15}$$

The complete shear stress with the heat flux (τ_w & q_w) of wall is illustrated bellow:

$$\left. \begin{aligned} \tau_w &= \left(\mu_{nf} \frac{\partial u}{\partial y} + \alpha_1 \left(u \frac{\partial^2 u}{\partial x \partial y} + 2 \frac{\partial u}{\partial y} \frac{\partial u}{\partial x} + v \frac{\partial^2 u}{\partial y^2} \right) \right)_{y=0}, \\ q_w &= -k_{hnf} \left(1 + \frac{16}{3} \frac{\sigma^* T_\infty^3}{\kappa^* \nu_f (\rho C_p)_f} \right) \left(\frac{\partial T}{\partial y} \right)_{y=0} \end{aligned} \right\} \tag{16}$$

Here, the reduced forms of physical industrial material with drag force and heat transfer rate is shown as:

$$\left. \begin{aligned} C_f \text{Re}_x^{\frac{1}{2}} &= \left(\frac{f''(0)}{\Phi_1} + \Gamma(3f''(0)f'(0) - f'''(0)f(0)) \right) \\ Nu_x \text{Re}_x^{-\frac{1}{2}} &= -\frac{k_{nf}}{k_f}(1 + Nr)\theta'(0). \end{aligned} \right\} \tag{17}$$

Here, local Nusselt numbers denoted by Nu_x and C_f represent the local skin friction coefficient. Finally, $\text{Re}_x = \frac{U_w x}{\nu_f}$ represents the local Reynolds number depending on the stretchable velocity ($U_w(x)$).

2.7. Entropy of System

The dimensionless system of entropy is described as:

$$N_G = \text{Re} \left(\Phi_5(1 + Nr)\theta'^2 + 1/\Phi_1 \cdot Br. / \Omega (f''^2 + Kf'^2) \right). \tag{18}$$

In which the Brinkman number is $Br = \omega_f U_w^2 / k_f (T_w - T_\infty)$, and $\Omega = T_w - T_\infty / T_\infty$ signifies the temperature gradient.

3. Numerical Algorithm (Shooting Scheme)

The flow system of ordinary differential Equations 10 and 11, under the specific boundary constraints 12, is solved numerically with the aid of the `bvp4c` method in MATLAB via the Lobatto-IIIa formula. For this phenomenon, firstly, the higher order ordinary differential equations are transmuted into first order ordinary differential equations (ODEs) with the help of innovative variables. Let

$$\begin{aligned} f &= s_1, \frac{df}{d\zeta} = s_2, \frac{d^2f}{d\zeta^2} = s_3, \frac{d^3f}{d\zeta^3} = s_4, \frac{d^4f}{d\zeta^4} = s'_4, \\ \theta &= s_5, \frac{d\theta}{d\zeta} = s_6, \frac{d^2\theta}{d\zeta^2} = s'_6, \end{aligned} \tag{19}$$

$$s'_4 = \frac{-A^2 + s_4 + \Phi_1 \left[\Phi_2(s_1s_3 - s_2^2) + \Gamma(2s_2s_4 - s_3^2) - \frac{Ks_2}{\Phi_1} \right]}{\Gamma\Phi_1s_1}, \tag{20}$$

$$s'_6 = \frac{-Pr \frac{\Phi_3}{\Phi_5} \left(s_1s_6 - s_2s_5 + \frac{Ec}{\Phi_1\Phi_3}s_3^2 + \frac{\Phi_4}{\Phi_3} M.Ec.s_2^2 \right)}{\left(1 + \frac{1}{\Phi_5} PrNr \right)}, \tag{21}$$

$$\begin{aligned} s_1(0) &= S, s_2(0) = 1, s_5(0) = 1, \\ s_2(\zeta) &\rightarrow A, s_3(\zeta) \rightarrow 0, s_5(\zeta) \rightarrow 0, \text{ as } \zeta \rightarrow \infty. \end{aligned} \tag{22}$$

Validation of Results

In this section, the validation of results is summarized. As shown in Table 3, we observed good agreement between published results and our current results.

Table 3. Validation of results in the case of pure fluid.

Γ	S	$C_f \text{Re}_x^{\frac{1}{2}}$		
		Rafiq et al. [31]	Jamshed et al. [32]	Current Results
0.0	0.5	-6.15999842542	-6.15983	-6.15982
0.2	0.5	-4.81951263596	-4.81947	-4.81945
0.5	0.0	-2.24678804753	-2.24666	-2.24664

4. Results and Discussion

The quantities significantly changed the behavior of flow through the desired domain. This section marks the parameters controlling characteristics of flow against flow and heat transfer of fluid. In the current article, a numerical solution is obtained by applying the *bvp4c* tool. Figures 2–8 examine the performance of parameters across subjective fields. The current results are compared with Rafiq et al. [31] and Jamshed et al. [32] as described in Table 3. Table 1 contains the thermophysical properties of solid particles and base fluid. The results are computed for an ample range of prominent parameters as $0.1 \leq S \leq 1.2$, $0.0 \leq A \leq 1.8$, $0.01 \leq \phi_1 = \phi_2 \leq 0.04$, $0.1 \leq Ec \leq 1.2$, $m = 3.0, m = 3.7, m = 4.6, m = 5.7$, $5.0 \leq Br \leq 20.0$, $5.0 \leq Re \leq 20.0$.

Figure 2 analyzes the effect of suction parameters via the velocity of fluid. It is visualized that the velocity profile is reduced for suction parameter values. Figure 3 is considered to show the behavior of the velocity ratio parameter against the fluid velocity profile. The growing estimations of the velocity ratio parameter result in an increment of velocity profile.

Figure 4 illustrates the nature of nanoparticle fraction on a thermal field of species. It is noted that the thermal distribution increases as the fraction of nanoparticles escalates. Figure 5 signifies the heat transfer field for increasing Eckert number. It is observed that larger values of the Eckert number boost the temperature of hybrid nanofluids. Physically, enhancement in the Eckert number improves the thermal state of fluid. Figure 6 examines the effect of velocity ratio parameter on thermal field. It can be noted that the temperature of fluid decreases when the values of the velocity ratio parameter are increased. Figure 7 illustrates the behavior of different shape factors, namely, sphere, bricks, tetrahedron and platelets, versus the temperature profile. It is noted that different variations of shape factors improve the energy profile of the hybrid nanofluid.

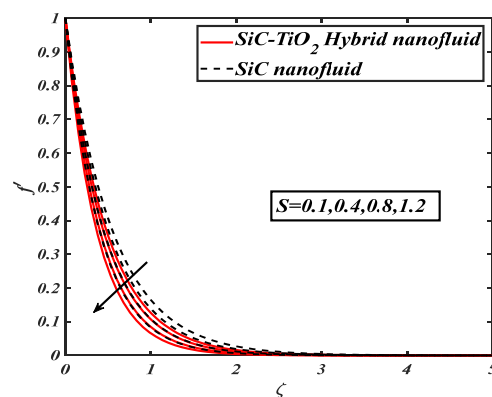


Figure 2. f' for varied S .

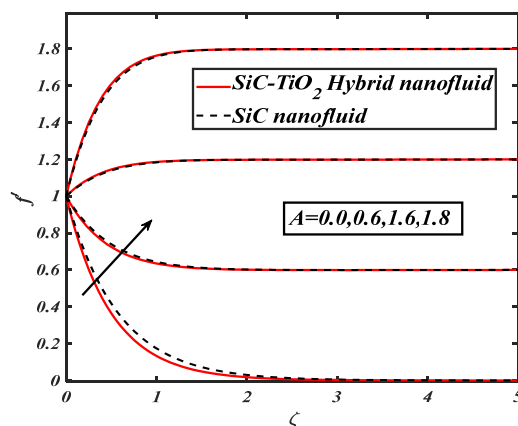


Figure 3. f' for varied A .

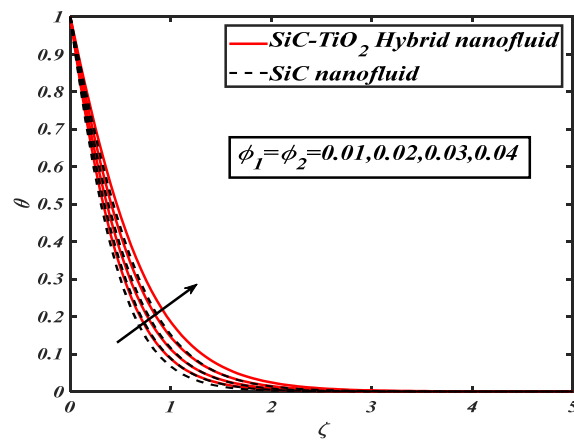


Figure 4. θ for varied ϕ, ϕ_1 .

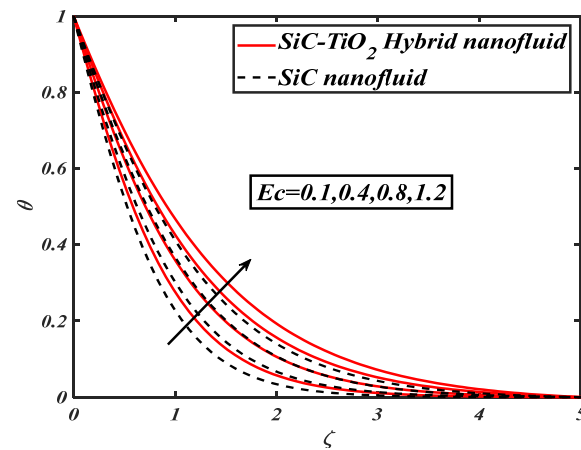


Figure 5. θ for varied Ec .

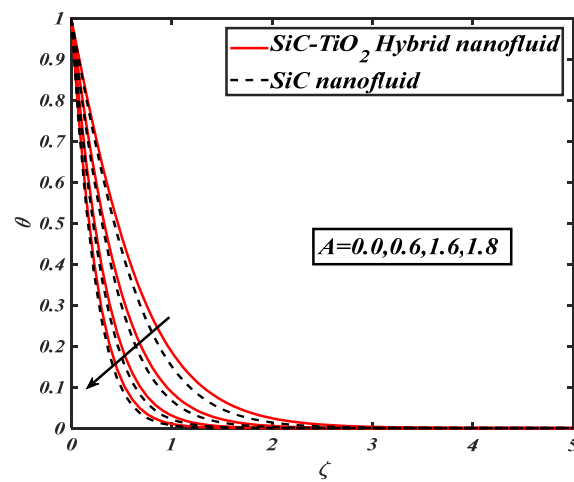


Figure 6. θ for varied A .

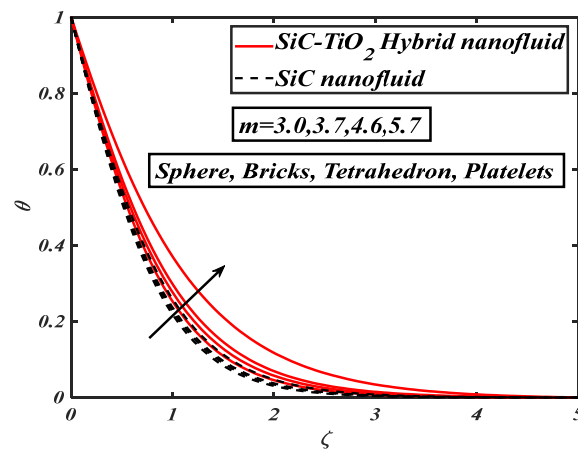


Figure 7. θ for different shapes factors.

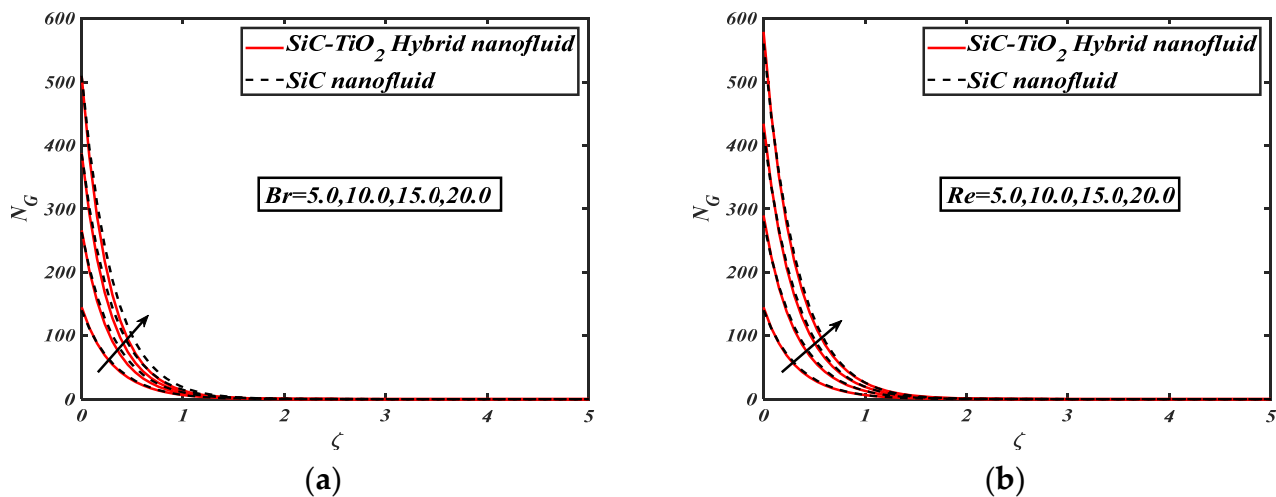


Figure 8. (a) N_G for varied Br , and (b) N_G for varied Re .

Figure 8a allows an inspection of the performance of the Brinkman number via an entropy generation field. Here, we suggest that entropy generation is boosted via the Brinkman number. The Brinkman number describes the viscosity and conductivity ratio among the medium, and heat variance between the surface and the ambient temperature. The entropy of system increases with increases in the medium conductivity via larger Brinkman numbers. Figure 8b indicates the trend in the Reynolds number via entropy generation. The entropy generation is an enhancing function of the Reynolds number. It is evident that the greater Reynolds number is due to a smaller viscous force that promotes the flow irreversibility of the structure.

5. Conclusions

Two-dimensional flow of kerosene oil in existence of SiC and TiO_2 nanoparticles past a moving flat horizontal surface with different shape effects and entropy production is studied numerically in this article. The tool of similarity transformations of variables is utilized to simplify flow governing the system of PDEs, and a *bvp4c* solver with the shooting technique utilized for solution development. The thermal profile of species improved with growing values of the Eckert number. The temperature profile escalated by enlarging the fraction of nanoparticles. The entropy production can be boosted with the enhancement of the Brinkmann parameter. The increment of Reynolds number augments the entropy production.

Author Contributions: Conceptualization, M.I.; methodology, M.I., S.Y. and H.W.; validation, M.I., S.Y. and H.W.; formal analysis, S.A.K. and T.M.; investigation, S.A.K. and T.M.; resources, T.M.; data curation, S.A.K., T.M. and N.A.; writing—original draft preparation, T.M. and N.A.; writing—review and editing, T.M., N.A., N.N.H. and I.K.; supervision, T.M.; project administration, T.M.; funding acquisition, T.M. and N.N.H. All authors have read and agreed to the published version of the manuscript.

Funding: The authors extend their appreciation to the Deanship of Scientific Research at King Khalid University, Abha, Saudi Arabia for funding this work through research groups program under grant number RGP.2/20/43 and The APC was funded by Nawaf N. Hamadneh.

Data Availability Statement: The data that support the findings of this study have not been made available but can be obtained from the author upon request.

Conflicts of Interest: The authors declare no conflict of interest.

Nomenclature

$(u&v)$	Velocity components [$m.s^{-1}$]
$(x&y)$	Cartesian coordinates [m]
(α_1, α_2)	Material constants
(U_w)	Stretching velocity [$m.s^{-1}$]
μ	Dynamic viscosity (kg/ms)
p	Pressure
$(A_{\zeta 1} & A_{\zeta 2})$	Rivlin–Erickson tensors
I	Identity tensor
$\frac{d}{dt}$	Time-dependent derivative
V	Velocity of fluid
ρ_{hnf}	Density of hybrid nanofluid (kg/m^3)
k_{hnf}	Thermal conductivity of hybrid nanofluid ($Wm^{-1}K^{-1}$)
$(\rho C_p)_{hnf}$	Hybrid nanofluid heat capacity ($Jm^{-3}K^{-1}$)
C_p	Specific heat (J/K)
q_r	Radiative heat flux (W/m^2)
B	Strength of Magnetic field [$N.m^{-1}.A^{-1}$]
σ^*	Stefan–Boltzmann constant
k^*	Mean absorption coefficient
Γ	Second grade fluid parameter
K	Porosity parameter
Nr	Thermal radiation parameter
Pr	Prandtl number
Ec	Eckert number
M	Magnetic parameter
S	Suction/injection velocity (ms^{-1})
A	Velocity ratio parameter
ϕ_1, ϕ_2	Volume fraction of nanoparticles
T_w	Temperature of the surface (K)
T_∞	Neighborhood temperature (K)
C_f	Coefficient of skin friction
Nu_x	Nusselt number
τ_w	Shear stress
q_w	Heat flux
Re_x	Local Reynolds number
Br	Brinkman number
Ω	Temperature gradient
N_G	Entropy generation
hnf	Thermophysical properties defined for hybrid nanofluid

References

1. Choi, S.U.; Eastman, J.A. *Enhancing Thermal Conductivity of Fluids with Nanoparticles*; FED; ASME: New York, NY, USA, 1995; Volume 66, pp. 99–105.
2. Rasool, G.; Shafiq, A.; Khaliq, C.M. Marangoni forced convective Casson type nanofluid flow in the presence of Lorentz force generated by Riga plate. *Discret. Contin. Dyn. Syst. S* **2021**, *14*, 2517. [[CrossRef](#)]
3. Mahanthesh, B.; Mackolil, J. Flow of nanofluid past a vertical plate with novel quadratic thermal radiation and quadratic Boussinesq approximation: Sensitivity analysis. *Int. Commun. Heat Mass Transf.* **2020**, *120*, 105040. [[CrossRef](#)]
4. Ramzan, M.; Shaheen, N.; Chung, J.D.; Kadry, S.; Chu, Y.-M.; Howari, F. Impact of Newtonian heating and Fourier and Fick's laws on a magnetohydrodynamic dusty Casson nanofluid flow with variable heat source/sink over a stretching cylinder. *Sci. Rep.* **2021**, *11*, 1–19. [[CrossRef](#)] [[PubMed](#)]
5. Eid, M.R.; Mabood, F. Thermal analysis of higher-order chemical reactive viscoelastic nanofluids flow in porous media via stretching surface. *Proc. Inst. Mech. Eng. Part C J. Mech. Eng. Sci.* **2021**, *235*, 6099–6110. [[CrossRef](#)]
6. Gowda, R.P.; Kumar, R.N.; Prasannakumara, B.; Nagaraja, B.; Giresha, B. Exploring magnetic dipole contribution on ferromagnetic nanofluid flow over a stretching sheet: An application of Stefan blowing. *J. Mol. Liq.* **2021**, *335*, 116215. [[CrossRef](#)]
7. Alsabery, A.; Tayebi, T.; Abosinnee, A.; Raizah, Z.; Chamkha, A.; Hashim, I. Impacts of Amplitude and Local Thermal Non-Equilibrium Design on Natural Convection within Nanofluid Superposed Wavy Porous Layers. *Nanomaterials* **2021**, *11*, 1277. [[CrossRef](#)]
8. Alsabery, A.; Hajjar, A.; Sheremet, M.; Ghalambaz, M.; Hashim, I. Impact of particles tracking model of nanofluid on forced convection heat transfer within a wavy horizontal channel. *Int. Commun. Heat Mass Transf.* **2021**, *122*, 105176. [[CrossRef](#)]
9. Khan, S.U.; Waqas, H.; Shehzad, S.A.; Imran, M. Theoretical analysis of tangent hyperbolic nanoparticles with combined electrical MHD, activation energy and Wu's slip features: A mathematical model. *Phys. Scr.* **2019**, *94*, 125211. [[CrossRef](#)]
10. Muhammad, T.; Waqas, H.; Khan, S.A.; Ellahi, R.; Sait, S.M. Significance of nonlinear thermal radiation in 3D Eyring–Powell nanofluid flow with Arrhenius activation energy. *J. Therm. Anal.* **2020**, *143*, 929–944. [[CrossRef](#)]
11. Shafiq, A.; Khan, I.; Rasool, G.; Sherif, E.-S.M.; Sheikh, A.H. Influence of Single- and Multi-Wall Carbon Nanotubes on Magnetohydrodynamic Stagnation Point Nanofluid Flow over Variable Thicker Surface with Concave and Convex Effects. *Mathematics* **2020**, *8*, 104. [[CrossRef](#)]
12. Waqas, H.; Yasmin, S.; Muhammad, T.; Imran, M. Flow and heat transfer of nanofluid over a permeable cylinder with nonlinear thermal radiation. *J. Mater. Res. Technol.* **2021**, *14*, 2579–2585. [[CrossRef](#)]
13. Hayat, T.; Muhammad, T.; Shehzad, S.A.; Alsaedi, A. Similarity solution to three dimensional boundary layer flow of second grade nanofluid past a stretching surface with thermal radiation and heat source/sink. *AIP Adv.* **2015**, *5*, 017107. [[CrossRef](#)]
14. Waqas, H.; Imran, M.; Muhammad, T.; Sait, S.M.; Ellahi, R. On bio-convection thermal radiation in Darcy–Forchheimer flow of nanofluid with gyrotactic motile microorganism under Wu's slip over stretching cylinder/plate. *Int. J. Numer. Methods Heat Fluid Flow* **2020**, *31*, 1520–1546. [[CrossRef](#)]
15. Wakif, A.; Chamkha, A.; Thumma, T.; Animasaun, I.L.; Sehaqui, R. Thermal radiation and surface roughness effects on the thermo-magneto-hydrodynamic stability of alumina–copper oxide hybrid nanofluids utilizing the generalized Buongiorno's nanofluid model. *J. Therm. Anal.* **2020**, *143*, 1201–1220. [[CrossRef](#)]
16. Hussain, A.; Hassan, A.; Al Mdallal, Q.; Ahmad, H.; Rehman, A.; Altanji, M.; Arshad, M. Heat transport investigation of magneto-hydrodynamics (SWCNT-MWCNT) hybrid nanofluid under the thermal radiation regime. *Case Stud. Therm. Eng.* **2021**, *27*, 101244. [[CrossRef](#)]
17. Kerschbaumer, N.M.; Niedermaier, S.; Lohmüller, T.; Feldmann, J. Contactless and spatially structured cooling by directing thermal radiation. *Sci. Rep.* **2021**, *11*, 16209. [[CrossRef](#)]
18. Alsabery, A.I.; Parvin, S.; Ghalambaz, M.; Chamkha, A.J.; Hashim, I. Convection Heat Transfer in 3D Wavy Direct Absorber Solar Collector Based on Two-Phase Nanofluid Approach. *Appl. Sci.* **2020**, *10*, 7265. [[CrossRef](#)]
19. Han, W.; Chen, X. Nano-electrokinetic ion enrichment in a micro-nanofluidic preconcentrator with nanochannel's Cantor fractal wall structure. *Appl. Nanosci.* **2019**, *10*, 95–105. [[CrossRef](#)]
20. Han, W.; Chen, X. A review: Applications of ion transport in micro-nanofluidic systems based on ion concentration polarization. *J. Chem. Technol. Biotechnol.* **2019**, *95*, 1622–1631. [[CrossRef](#)]
21. Waqas, H.; Khan, S.A.; Khan, S.U.; Khan, M.I.; Kadry, S.; Chu, Y.-M. Falkner-Skan time-dependent bioconvection flow of cross nanofluid with nonlinear thermal radiation, activation energy and melting process. *Int. Commun. Heat Mass Transf.* **2020**, *120*, 105028. [[CrossRef](#)]
22. Han, W.; Chen, X. Nano-electrokinetic ion enrichment of highly viscous fluids in micro-nanochannel. *Chem. Eng. Process. Process Intensif.* **2019**, *143*, 107626. [[CrossRef](#)]
23. Eid, M.R.; Mabood, F. Two-phase permeable non-Newtonian cross-nanomaterial flow with Arrhenius energy and entropy generation: Darcy-Forchheimer model. *Phys. Scr.* **2020**, *95*, 105209. [[CrossRef](#)]
24. Eid, M.R.; Mabood, F. Entropy analysis of a hydromagnetic micropolar dusty carbon NTs-kerosene nanofluid with heat generation: Darcy–Forchheimer scheme. *J. Therm. Anal.* **2021**, *143*, 2419–2436. [[CrossRef](#)]
25. Turkyilmazoglu, M. Velocity Slip and Entropy Generation Phenomena in Thermal Transport Through Metallic Porous Channel. *J. Non-Equilib. Thermodyn.* **2020**, *45*, 247–256. [[CrossRef](#)]

26. Shehzad, S.A.; Madhu, M.; Shashikumar, N.S.; Gireesha, B.J.; Mahanthesh, B. Thermal and entropy generation of non-Newtonian magneto-Carreau fluid flow in microchannel. *J. Therm. Anal.* **2020**, *143*, 2717–2727. [[CrossRef](#)]
27. Hayat, T.; Haider, F.; Alsaedi, A.; Ahmad, B. Entropy generation analysis of Carreau fluid with entire new concepts of modified Darcy's law and variable characteristics. *Int. Commun Heat Mass Transf.* **2021**, *120*, 105073. [[CrossRef](#)]
28. Shah, Z.; Alzahrani, E.O.; Dawar, A.; Alghamdi, W.; Ullah, M.Z. Entropy Generation in MHD Second-Grade Nanofluid Thin Film Flow Containing CNTs with Cattaneo-Christov Heat Flux Model Past an Unsteady Stretching Sheet. *Appl. Sci.* **2020**, *10*, 2720. [[CrossRef](#)]
29. Jawad, M.; Saeed, A.; Tassaddiq, A.; Khan, A.; Gul, T.; Kumam, P.; Shah, Z. Insight into the dynamics of second grade hybrid radiative nanofluid flow within the boundary layer subject to Lorentz force. *Sci. Rep.* **2021**, *11*, 4894. [[CrossRef](#)]
30. Brewster, M.Q. *Thermal Radiative Transfer and Properties*; John Wiley & Sons: Hoboken, NJ, USA, 1992.
31. Rafiq, M.; Kamran, M.; Ahmed, N.; Mohyud-Din, S.T.; Bashir, Y.; Haider, S.A.; Farwa, S.; Tahir, M. Analytical solution for the flow of second grade fluid over a stretching sheet. *AIP Adv.* **2019**, *9*, 055313. [[CrossRef](#)]
32. Jamshed, W.; Mishra, S.; Pattnaik, P.; Nisar, K.S.; Devi, S.S.U.; Prakash, M.; Shahzad, F.; Hussain, M.; Vijayakumar, V. Features of entropy optimization on viscous second grade nanofluid streamed with thermal radiation: A Tiwari and Das model. *Case Stud. Therm. Eng.* **2021**, *27*, 101291. [[CrossRef](#)]